Korean J. Chem. Eng., 34(11), 2922-2932 (2017)
DOI: 10.1007/s11814-017-0181-3

pISSN: 0256-1115
eISSN: 1975-7220

Adsorption and desorption dynamics of CF_4 on activated carbon beds: Validity of the linear driving force approximation for pressure-changing steps

Dong-Woo Cho, Won Sik Kim, Heynsung Chang, Tae Sung Jung, Jongkee Park, and Jong-ho Park†

Clean Fuel Laboratory, Climate Change Research Division, Korean Institute of Energy Research,
152 Gajeong-ro, Yuseong-gu, Daejeon 34129, Korea
(*Received 22 December 2016 • accepted 2 July 2017*)

Abstract−Adsorption and desorption dynamics of CF_4 on an activated carbon bed were studied experimentally and theoretically, focusing on pressure-changing steps. The theoretical model used the ideal adsorbed solution (IAS) theory and the linear driving force (LDF) approximation as equilibrium and mass transfer models, respectively. Adsorption breakthrough curves of raw CF_4 gas (500, 1,000, and 1,500 ppm) were well predicted by the theoretical model and the diffusion time constant for CF_4 was found to be 3.3×10^{-3} s^{-1} from breakthrough curve fitting. Changes in the CF_4 concentration during depressurization could be easily predicted using the above mathematical model when the half-cycle time (θ_c) was above 0.1. However, significant discrepancies were observed between the predicted CF_4 concentrations and the experimental data when θ_c was 0.1. Nakao and Suzuki also reported that proportional constant of LDF approximation ($=KD_e/R_p^2$) needs to be modified when θ_c is less than 0.1.

Keywords: Adsorption, Desorption, PFC, CF_4, Activated Carbon, Linear Driving Force

INTRODUCTION

Perfluorocarbons (PFCs) are widely used in the semiconductor industry for cleaning and other purposes, possessing extremely high global warming potentials that are thousands to tens of thousands times higher than that of CO_2. Accordingly, PFCs are controlled under the Kyoto Protocol, with global efforts made to reduce their emissions.

Carbon tetrafluoride (CF_4) is a PFC widely used for cleaning in chemical vapor deposition and semiconductor etching processes, having a global warming potential approximately 5,700 times higher than that of CO_2 and an atmospheric lifetime of ~50,000 years. Methods of reducing CF_4 emissions include oxidative decomposition (e.g., combustion), catalytic and plasma oxidation, recycling through reclamation and concentration, and substitution with alternative compounds.

Hou et al. [1] reported PFC decomposition by dielectric barrier discharge plasma, while Marilena [2] studied CF_4 decomposition by microwave plasma and reported that 98% of CF_4 in raw gas (flow of 16 L/min) could be decomposed using a power of 1.9 kW. How and Rung [3] conducted a study of CF_4 decomposition using tandem packed-bed plasma (TPBP) and Sun and Park [4] conducted a study of CF_4 decomposition by thermal plasma processing.

Among the above methods, decomposition of PFCs by combustion is the one most extensively studied. PFC combustion systems using natural gas or hydrogen fuels exhibit decomposition efficiencies above 90% for compounds such as C_2F_6 and NF_3. However, CF_4 is reported to have a low decomposition rate due to the considerably high C-F bond energy of 486 kJ/mol.

The disadvantages of the combustion method include excessive amounts of fuel required for decomposition and high operating costs, since the generated HF needs to be removed by scrubbing. Numerous catalytic oxidation studies have been conducted to overcome these shortcomings, e.g., Takita et al. [5] reported that CF_4 can be decomposed at 973 K using mixed aluminum phosphate and rare earth metal phosphate catalysts. However, this process faces the problem of high-temperature catalyst stability due to the formation of HF in the decomposition reaction. Xua et al. [6] studied the oxidative decomposition of CF_4 using an alumina catalyst and investigated the hydrolytic decomposition of CF_4 using an alumina catalyst supported on metal oxides (e.g., potassium and copper oxides).

The decomposition of CF_4 by both plasma treatment and high-temperature combustion (above 1,600 °C) requires a large supply of electrical energy and fuel, increasing operating costs. Therefore, finding ways to reduce energy consumption is important for making these processes economically feasible. Generally, the level of PFC emission from the electronics industry corresponds to several hundreds to several thousands of ppm. The emitted PFCs contain an excessive amount of nitrogen, since it is used for cleaning at the front end of vacuum pumps in chemical deposition and etching processes.

In the combustion process, large amounts of energy are required to raise the temperature of the excess N_2, since the temperature of PFCs can be raised only by simultaneously heating nitrogen. For plasma treatment, more free radicals are required to process diluted PFCs, leading to a larger consumption of electricity. Thus, enrichment of PFCs can greatly contribute to reducing the energy consumption of PFC decomposition via combustion or plasma treatment.

PFCs diluted by nitrogen has been concentrated by using mem-

†To whom correspondence should be addressed.
E-mail: jongho@kier.re.kr

brane- and adsorbent-based gas separation technologies [7,8], with the adsorption process exhibiting significant advantages such as the use of simple apparatus and ease of operation. These advantages have already been utilized in the separation of oxygen from air [9,10] and hydrogen from petrochemical emission gases [11-13]. Adsorption-based separation processes can be classified as either pressure swing adsorption (PSA) or thermal swing adsorption (TSA), depending on how the adsorbent is regenerated [14].

PSA features adsorption at high pressure, with desorption performed by lowering the pressure. Therefore, the PSA process includes pressurization and depressurization of the adsorption bed, with parameters determined by the number of adsorption beds and the purpose of this process. Since these pressurization and depressurization steps significantly influence the overall process performance, an accurate understanding of PSA adsorption and desorption dynamics is crucial for the design and optimization of this method.

Since PSA is extensively used in various industries, numerous mathematical models have been developed to describe its dynamics, being based on mass balance and energy balance equations and adopting various forms depending on the adsorption equilibrium, heat transfer rate, and mass transfer rate equations [15]. For porous adsorbents, a simple linear driving force (LDF) approximation is commonly used as the mass transfer rate equation instead of the diffusion equation. The LDF approximation was first proposed by Glueckauf [16], and its simplicity has led to its extensive use for analyzing the PSA process. Furthermore, many studies were performed to overcome the limitations of the LDF approximation. Nakao and Suzuki [17] studied the mass transfer coefficient (MTC) changes in different adsorption and desorption cycles using a single adsorbent. Alpay et al. [18] used theoretical analysis to numerically calculate MTCs in cases where the half-cycle time of adsorption and desorption is short compared to the diffusion time constant ($q_c=t_c(D_e/R_p^2)<0.1$). Raghavan et al. [19] investigated the effects of adsorption isotherm non-linearity on the MTC, whereas Liaw et al. [20] demonstrated that the MTC initially proposed by Glueckauf ($k=15(D_e/R_p^2)$) is obtained when the adsorbate concentration within the adsorbent can be approximated with a quadratic equation. Do and Mayfield [21] expanded Liaw's study by deriving the MTC with the help of concentration distribution equations with degrees higher than two, and Kim et al. [22] proposed an improved LDF approximation method, taking into account that the adsorbent surface boundary conditions change with time.

Confirming the validity of the LDF approximation during PSA pressurization and depressurization steps is required for the use of mathematical analysis to understand the performance of this process. The aforementioned studies have also attempted to expand the applicability and validity of the LDF approximation for cyclic adsorption and desorption; however, its applicability was investigated using the frozen solid approximation, which assumes that adsorbate adsorption and desorption do not occur during pressurization and depressurization [14].

Tondeur et al. [23] studied the suitability of the LDF mass transfer approximation by comparing simulated concentration distributions of adsorbates obtained using diffusion and LDF models for pressure-changing pressurization and depressurization steps. LDF approximation applicability by actual testing has usually been confirmed by using an indirect method for predicting pressure changes in the adsorption bed during pressurization and depressurization [23-26]. Todd and Webley [27] compared and verified LDF and diffusion models for a short-cycle oxygen separation process and used an indirect method to compare the corresponding performances for determining the accuracy of the LDF model.

Pressurization and depressurization in actual PSA processes greatly influence their performance. However, experimental and theoretical studies analyzing the adsorption and desorption dynamics of this process are scarce. Here, we studied the adsorption and desorption dynamics of CF_4 on activated carbon experimentally and theoretically as a pre-step to designing an adsorption process for the selective removal of CF_4 from a mixture of CF_4/N_2. In particular, adsorption and desorption dynamics were studied for pressure-changing steps, which are important for the PSA process, with the accuracy of the LDF approximation also investigated.

EXPERIMENTAL

1. Materials

CF_4 (99.9 vol%) and nitrogen (99.99 vol%) were used for single-component adsorption equilibrium measurements. For adsorption and desorption breakthrough tests, extra pure N_2 (99.999%) and mixed gas (1 vol% CF_4 in N_2) were used. All gases were obtained from Special Gas Co., Ltd. Commercially available coconut shell (WSC-470)-based activated carbons purchased from the Calgon Carbon Corporation were used as adsorbents.

2. Single-component Adsorption Equilibria of CF_4 and N_2

Single-component adsorption equilibria of CF_4 and nitrogen on activated carbons (WSC-470) were characterized using a volumetric adsorption equilibrium apparatus (BELSORP mini, BEL Japan, Inc., Japan). Experiments were conducted at pressures of 0-1 atm and temperatures of 10, 25, 40, and 60 °C.

3. Adsorption and Desorption Breakthrough Tests

Adsorption and desorption breakthrough experiments were performed using the apparatus shown in Fig. 1. A stainless steel tube with a length of 100 cm and an inner diameter of 13 cm filled with 6.5 kg of adsorbent was used as an adsorption column. A mass flow controller (MFC) was installed to control the supply of mixed and desorption gases, and thermocouples were placed 10, 30, 50, 70, and 90 cm from the bottom of the adsorption bed to measure the temperature changes inside it. A back pressure regulator (BPR) was installed on the upper part of the adsorption bed to maintain the pressure within the bed constant during adsorption. Pressure changes were measured using a pressure gauge installed on the upper part of the bed. The concentration of CF_4 in the feed was controlled by mixing pure nitrogen (99.999%, obtained by vaporizing liquid nitrogen) and the mixed gas (1 vol% CF_4 in N_2, sourced from a commercial supplier). A vacuum pump (Edwards XDS35i) was connected to the bottom of the adsorption bed to enable the investigation of desorption characteristics under vacuum. The composition of gases emitted during the adsorption experiment was measured in real time using a quadrupole mass spectrometer (OmniStar GSD 301 O_2).

Adsorption and desorption experiments were performed in the following manner. Prior to the adsorption experiment, the adsor-

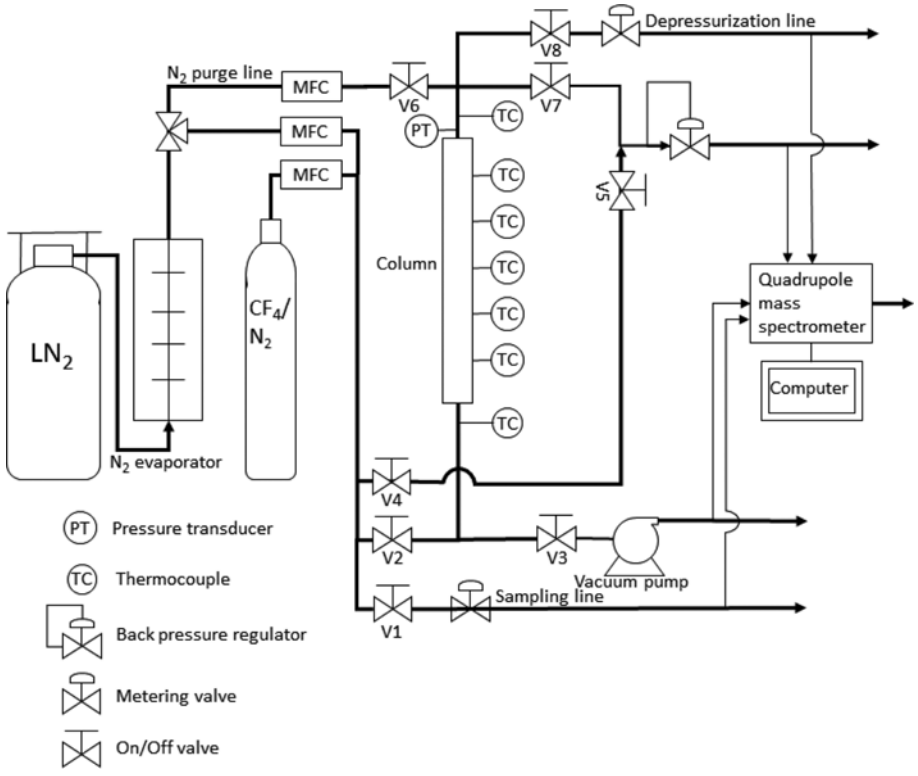

Fig. 1. Schematic diagram of the apparatus used for breakthrough experiments.

bent was regenerated for 5 h with pure nitrogen supplied at 20 L/min under vacuum (0.05 atm). Once the regeneration process was completed, the back pressure was controlled to raise the desired pressure within the adsorption bed, while N_2 was supplied at 200 L/min. As the pressure was raised, the temperature inside the adsorption bed, which had risen due to the adsorption of nitrogen, was lowered to room temperature using a sufficient amount of supplied N_2. After the adsorption bed was sufficiently saturated with nitrogen gas at room temperature, the valves on its top and bottom were shut off.

Before the adsorption experiment, the flows of N_2 and CF_4 were adjusted using the MFC to obtain the desired mixture composition. The composition was monitored using the mass spectrometer by passing the gas through the analysis line (V1 valve (Fig. 1) opened; flow controlled using the metering valve). Subsequently, breakthrough experiments were conducted by passing the mixed gas over the adsorption bed that was completely regenerated.

To investigate the adsorption and desorption dynamics in the pressure-changing steps of the PSA process, N_2/CF_4 mixed gas was supplied until full adsorbent saturation. The adsorption bed saturated with N_2/CF_4 at a given pressure was depressurized to 1 atm by opening the V8 valve, with depressurization time controlled by a metering valve located behind the V8 valve. The changes in CF_4 concentration during depressurization were analyzed by a mass spectrometer, with samples supplied using the depressurization line.

The following experiment was performed to examine the desorption characteristics of CF_4 in vacuum. The adsorption bed was saturated with N_2/CF_4 (1,000 ppm of CF_4) at room temperature and a pressure of 3.2 atm. Subsequently, the V8 valve was opened for 30 s to lower the pressure to 1 atm. Then, the V3 valve was opened for depressurization using a vacuum pump, and the V6 valve was simultaneously opened for nitrogen purging. Purging was performed at 40 and 60 L/min until CF_4 was completely desorbed, and the changes in CF_4 concentration were analyzed using a mass spectrometer.

THEORETICAL BACKGROUND

To simulate adsorption bed dynamics, a system of related equations must be solved, such as the adsorption bed mass balance, energy balance, adsorption rate within the adsorbent, as well as the adsorption equilibrium for predicting adsorption isotherms. The following assumptions were made in the employed mathematical model:

(1) All gases used are ideal gases.

(2) Diffusion in the axial direction and the radial gradients of flow rate, concentration, and temperature can be ignored.

(3) The adsorption rate is modeled by the LDF equation, featuring a linear dependence on the adsorption amount.

(4) The adsorbent physical properties and rate equation parameters are virtually unaffected by temperature.

Based on these assumptions, the mass balance equations for all mixed gas components and the overall mass balance equation can be expressed as follows.

Mass balance equation for individual components:

$$\frac{\partial C_{y_i}}{\partial t} + \frac{\partial (uC_{y_i})}{\partial z} + \frac{(1-\varepsilon)}{\varepsilon}\rho_p \frac{\partial \bar{q}_i}{\partial t} = 0 \quad (1)$$

Overall mass balance equation:

$$\frac{\partial C}{\partial t}+\frac{\partial(uC)}{\partial z}+\Sigma_i\frac{1-\varepsilon}{\varepsilon}\rho_p\frac{\partial \bar{q}_i}{\partial t}=0 \tag{2}$$

When heat transfer to the adsorption bed wall is taken into account, the atmospheric heat balance equation is expressed as follows:

$$(\varepsilon c_{pg}C+(1-\varepsilon)c_{ps}\rho_p)\frac{\partial T}{\partial t}+\varepsilon c_{pg}uC\frac{\partial T}{\partial z} -\Sigma_i(-\Delta H_a)(1-\varepsilon)\ \rho_p\frac{\partial q_i}{\partial t}+\frac{2h_w}{R_i}(T-T_w)=0 \tag{3}$$

In Eq. (3), the last term represents heat transfer to the adsorption bed wall, and the corresponding heat balance can be expressed as:

$$c_{pw}\rho_w\alpha_w\frac{\partial T_w}{\partial t}=2\pi h_w R_i(T-T_w)-2\pi U_w R_0(T_w-T_F) \tag{4}$$

The LDF model representing the rate of mass transfer to the adsorbent can be expressed as:

$$\frac{\partial q_i}{\partial t}=k_i(q_i^*-\bar{q}_i) \tag{5}$$

Glueckauf [16] claimed that the overall MTC is proportional to $15(D_e/R_p^2)$.

Multicomponent adsorption equilibria were modeled using the IAS theory, which can predict these equilibria based on pure-component adsorption equilibrium data. This theory is well suited for multicomponent adsorption equilibria, particularly for those of hydrocarbons. Although numerous types of pure-component adsorption equilibria can be used in the IAS theory, we used the simplest adsorption equilibrium model, the Langmuir model, which can be expressed as:

$$q_i=\frac{q_{si}b_iP_i}{1+b_iP_i} \tag{6}$$

where b_i and q_{si} are parameters related to the adsorption intensity and amount of adsorbate at saturation, respectively, with their temperature dependences given by:

$$b_i=b_{io}\exp(b_{i1}/T) \text{ and } q_{si}=a_{i,1}+q_{i,2}/T \tag{7}$$

The pressure drop within the adsorption bed was calculated using the Ergun equation:

$$\frac{\partial P}{\partial Z}=-K_1u-K_2u^2 \tag{8a}$$

$$K_1=\frac{150\mu(1-\varepsilon)^2}{d^2P\quad\varepsilon^3},\ K_2=1.75\rho_g\frac{1-\varepsilon}{d_p\varepsilon^3} \tag{8b}$$

The following boundary conditions were used.

Adsorption:

$$y_i(0,t)=y_{i,F},\ T(0,t)=T_F,\ u(0,t)=u_H,\ P(L,t)=P_{ad} \tag{9}$$

Depressurization:

$$u(L,t)=u_D=C_v\times(P_{z=L}-P_{atm})^n,\ u(0,t)=0,\ P(L,t)=P_{atm} \tag{10}$$

Vacuum cleaning:

$$y_i(L,t)=y_{i,db},\ T(L,t)=T_F,\ u(L,t)=u_{PL},\ u(0,t)=u_{wa},\ P(L,t)=P_{atm} \tag{11}$$

Table 1 lists the physical properties of the adsorption bed and adsorbent used in this study and the values of parameters used in the corresponding simulations.

Table 1. Physical properties of the used adsorption bed and adsorbent and parameters used in the corresponding simulations

Physical properties of bed and adsorbents		
Bed inner diameter	[cm]	13
Bed outer diameter	[cm]	13.5
Bed height	[cm]	100
Bed porosity	[-]	0.36
Particle density	[g/cm^3]	0.82
Particle diameter	[cm]	0.3
Wall density	[g/cm^3]	8.0
Gas heat capacity	[cal/(mol·K)]	6.95
Adsorbent heat capacity	[cal/(g·K)]	0.23
Wall heat capacity	[cal/(g·K)]	0.11
Mass and heat transfer coefficients		
h_w [cal/(cm^2·s·K)]		2.1×10^{-4}
U_w [cal/(cm^2·s·K)]		1.87×10^{-4}
k_{N2} [s^{-1}]		0.5
k_{CF4} [s^{-1}]		0.05

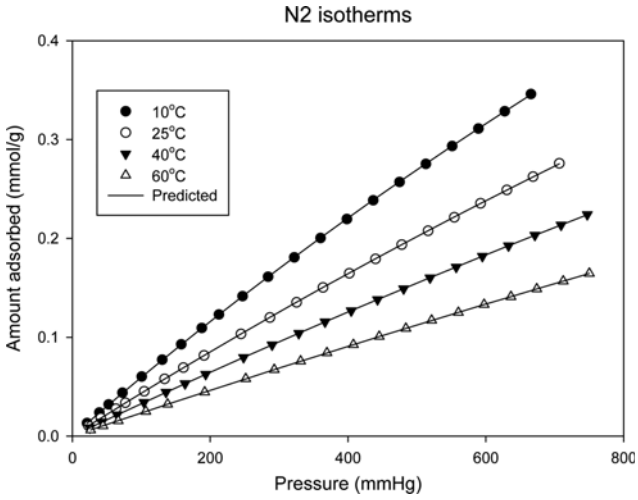

Fig. 2. Adsorption isotherms of N_2 on activated carbon.

RESULTS AND DISCUSSION

1. Adsorption Equilibrium

Figs. 2 and 3 compare the adsorption isotherms of N_2 and CF_4 on activated carbon, respectively, with the simulated results (Langmuir model). As is evident from these figures, activated carbon adsorbed CF_4 in preference to N_2. The adsorption of these species followed the general trends of physical adsorption, with the amount of adsorbate increasing with increasing pressure and decreasing with increasing temperature. The obtained results confirm that these adsorption equilibria were successfully simulated by the Langmuir model, with the corresponding equilibrium constants listed in Table 2. These values were used to calculate the selectivity of CF_4 adsorption, which was maximal at 25 °C and minimal at 60 °C. The mean

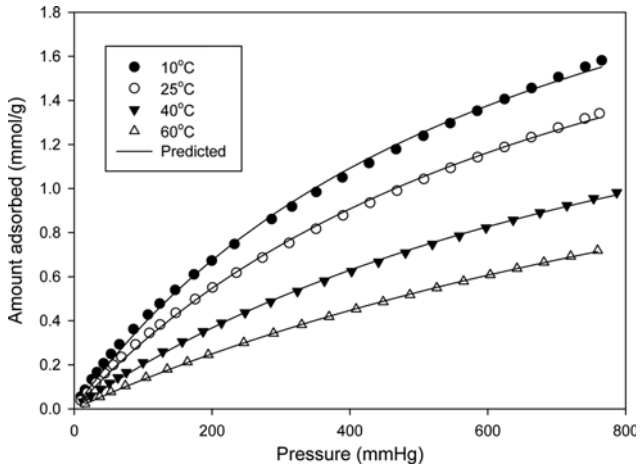

Fig. 3. Adsorption isotherms of CF_4 on activated carbon.

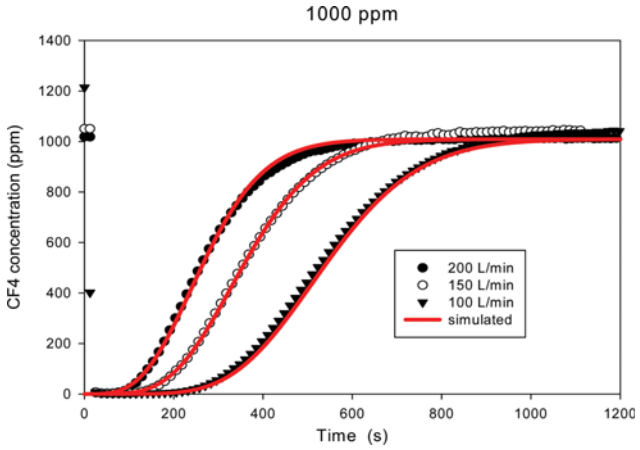

Fig. 4. Breakthrough curves of CF_4 at different feed flow rates (adsorption pressure, 3 atm; temperature, 293 K).

Table 2. Langmuir isotherm parameters and heats of adsorption

	$a_{i,1e}$ [mol/g]	$a_{i,2}$ [mol·K/g]	$b_{i,0}\times10^7$ [$mmHg^{-1}$]	$b_{i,1}$ [K]	$-\Delta H_a$ [kcal/mol]
N_2	2.323	0.0	4.737	1787	3.542
CF_4	−2.506	1.52	60.191	1583	5.399

Table 3. Langmuir isotherm parameters

Temperature [K]		q_s [mmol/g]	b [$mmHg^{-m}$]	$(q_s\times b)_{CF_4}/(q_s\times b)_{N_2}$
283.15	N_2	2.323	2.624×10^{-4}	7.24
	CF_4	2.870	1.537×10^{-3}	
293.15	N_2	2.323	1.903×10^{-4}	7.79
	CF_4	2.663	1.293×10^{-3}	
313.15	N_2	2.323	1.428×10^{-4}	6.64
	CF_4	2.208	9.980×10^{-4}	
353.15	N_2	2.323	1.016×10^{-4}	6.00
	CF_4	2.126	6.659×10^{-4}	

deviation between the predicted values and experimental results equaled 0.34% for N_2 and 5.7% for CF_4. The adsorption heats of CF_4 and N_2 were calculated using the Clausius-Clapeyron equation. The loading ratio correlation (LRC) was used to predict the adsorbate amount, being a non-iterative method and giving better predictions than the Langmuir model. The adsorption heats of N_2 and CF_4 derived from adsorption isotherms equaled 3.542 and 5.399 kcal/mol, respectively.

2. Fixed Bed Adsorption Experiments

Fig. 4 displays the experimentally determined (feed flow rates of 100, 150, and 200 L/min, pressure of 3 atm, CF_4 concentration of 1,000 ppm) and simulated breakthrough curves. Accurate predictions of binary adsorption equilibria are required to predict the adsorption dynamics. As mentioned, the binary adsorption equilibria in this study were modeled using the IAS theory based on pure-component adsorption equilibria of N_2 and CF_4 as long as it was possible. As shown in Fig. 4, the simulated breakthrough curves well matched the experimental ones for all feed flow rates, confirming that the IAS theory could accurately model the adsorption

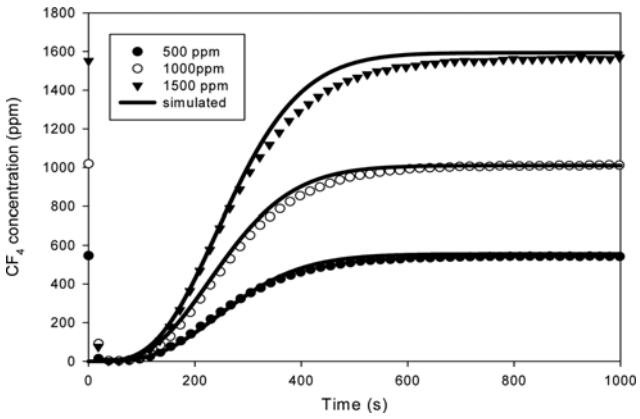

Fig. 5. Effect of CF_4 concentration in the feed on breakthrough curves (feed flow rate, 200 /min; adsorption pressure, 3 atm).

equilibrium of CF_4 in the CF_4/N_2 binary system. Although not shown in the figure, hardly any temperature changes were observed in the bed during the adsorption experiment, indicating that the concentration of adsorbed CF_4 was low even at 1,000 ppm, just as the corresponding heat of adsorption was.

The time required for the concentration of CF_4 in the downstream emission gas to drop to 10 ppm at N_2 flow rates of 100, 150, and 200 L/min was 217, 130, and 83 s, respectively. Operating a continuous CF_4 concentration process requires keeping the amount of CF_4 emissions into the atmosphere to a minimum. Therefore, the adsorption time for a continuous process must be shorter than the aforementioned adsorption breakthrough time.

Fig. 5 shows the adsorption breakthrough curves for CF_4 concentrations of 500, 1,000, and 1,500 ppm at a feed flow rate of 200 L/min and an adsorption pressure of 3 atm. The simulated results (also displayed in this figure) accurately predicted the experimental breakthrough curves, confirming that the IAS theory can accurately predict binary adsorption equilibria of CF_4 in different concentration ranges. As shown in the figure, the stages of major CF_4 mass transfer and the early breakthrough times for CF_4 concentrations of 500, 1,000, and 1,500 ppm were almost identical for both

simulated and experimental results, indicating that the experimental CF_4 transfer velocity within the adsorption bed (velocity of the CF_4 concentration wave front) was constant and independent of the CF_4 concentration.

3. Depressurization Experiments and Data Correlation

During PSA, the adsorbent is regenerated by changing the pressure; therefore, this process must include a depressurizing step following adsorption. For this reason, an accurate understanding of the corresponding adsorption and desorption dynamics is important for predicting the performance of continuous processes. For the depressurization experiment performed in this study, the adsorption bed was saturated with feed components at a given pressure, with depressurization rates subsequently modified to study changes in the emitted gas composition.

The adsorbent was saturated with CF_4 by supplying mixed gas with a CF_4 concentration of 1,000 ppm for a sufficient amount of time at an adsorption pressure of 3 atm. Subsequently, the adsorption bed was depressurized to atmospheric temperature within ~2 min, with the corresponding pressure and temperature changes shown in Figs. 6(a) and 6(b), respectively. Since depressurization was achieved by opening a valve to atmosphere, the pressure dropped rapidly at an early stage due to the large pressure difference, slowing down as this difference decreased. For an accurate simulation of this process, it was necessary to describe precisely the gas flow change through the valve. In general, this change was estimated using flow coefficient, as follows:

$$Q = C_v \times \sqrt{\frac{\Delta P}{SC}} \tag{12}$$

However, as shown in Eq. (10), the gas flow rate during depressurization was assumed to be proportional to n.

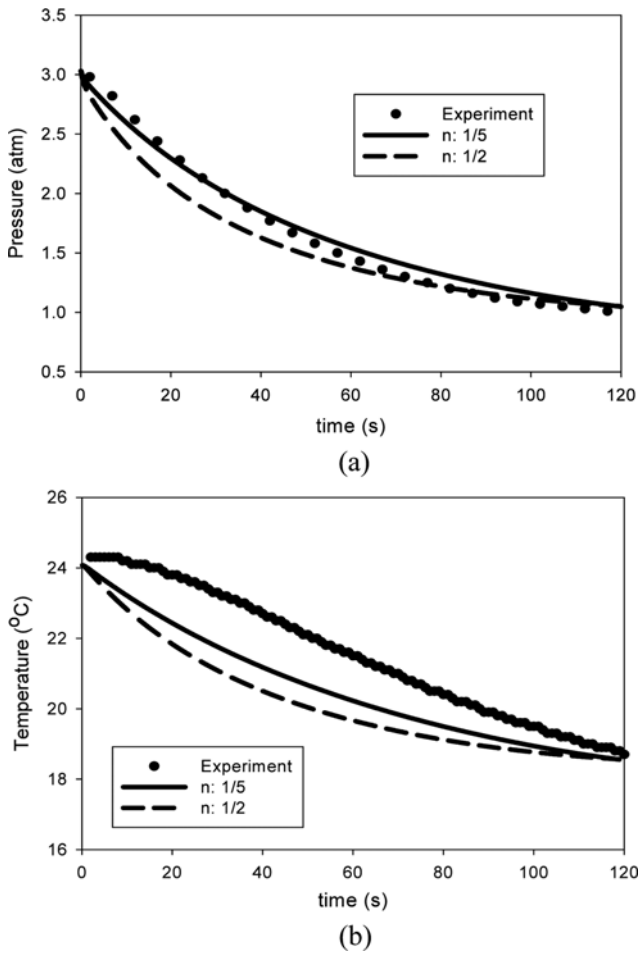

Fig. 6. Experimental and simulated (a) pressure and (b) temperature evolution during 2-min depressurization. Simulation was performed with two different n values (Eq. (10)).

Fig. 6(a) shows the results of simulating pressure changes using Eq. (10), demonstrating that pressure changes were predicted more accurately by n=1/5 than by n=1/2. In the latter case, the early stage pressure drop was more rapid than that observed experimentally. However, as the pressure approached 1 atm, the corresponding change was slower than the experimentally observed one. On the other hand, for n=1/5, the pressure decrease was slow in the early depressurization stage, with the overall trend being similar to experimental results. Based on this, it was concluded that Eq. (12) was suitable for predicting the gas flow rate at both ends of the valve, not being able to describe rapid pressure changes.

Fig. 6(b) shows the experimental temperature changes within the adsorption bed during depressurization to atmospheric pressure, together with the simulated results. During a 2-min depressurization experiment, the adsorption bed temperature decreased almost linearly. However, for n=1/2, a greater amount of nitrogen was desorbed due to the more rapid pressure decrease at the early depressurization stage. Consequently, the temperature decrease within the adsorption bed was faster than that observed experimentally. Moreover, as the pressure approached 1 atm, the rate of pressure change decreased, decreasing the amount of desorbed N_2 and the rate of adsorption bed temperature change. On the other hand, for n=1/5, the slow initial depressurization rate caused a slower decline of the adsorption bed temperature compared to the case of n=1/2. However, although the pressure change trend was more accurately predicted by n=1/5, the corresponding temperature decrease at the early depressurization stage was faster than that observed experimentally, slowing down as the pressure approached 1 atm. As shown in Fig. 6(b), the experimentally determined and simulated final temperatures were very similar at the end of depressurization. Therefore, simulations were performed assuming that the flow rate through the valve during depressurization was proportional to the pressure difference raised to the power of 1/5.

Fig. 7(a) shows experimental and simulated CF_4 concentration changes for depressurization from 3.0 atm to atmospheric pressure. Experimental CF_4 concentrations increased almost linearly as the adsorption bed pressure decreased with time, reaching ~1,940 ppm when depressurization was close to completion. The increase in the CF_4 concentration during depressurization was due to its high adsorption selectivity, resulting in a greater amount of CF_4 being desorbed per unit pressure change, compared to that of nitrogen. The simulated CF_4 concentration increased almost linearly with time and was accurately predicted for the initial depressurization stage. According to the results shown in Fig. 7(a), the simulated CF_4 concentrations accurately reproduced experimental results for approximately the first 60 s of depressurization, subsequently drop-

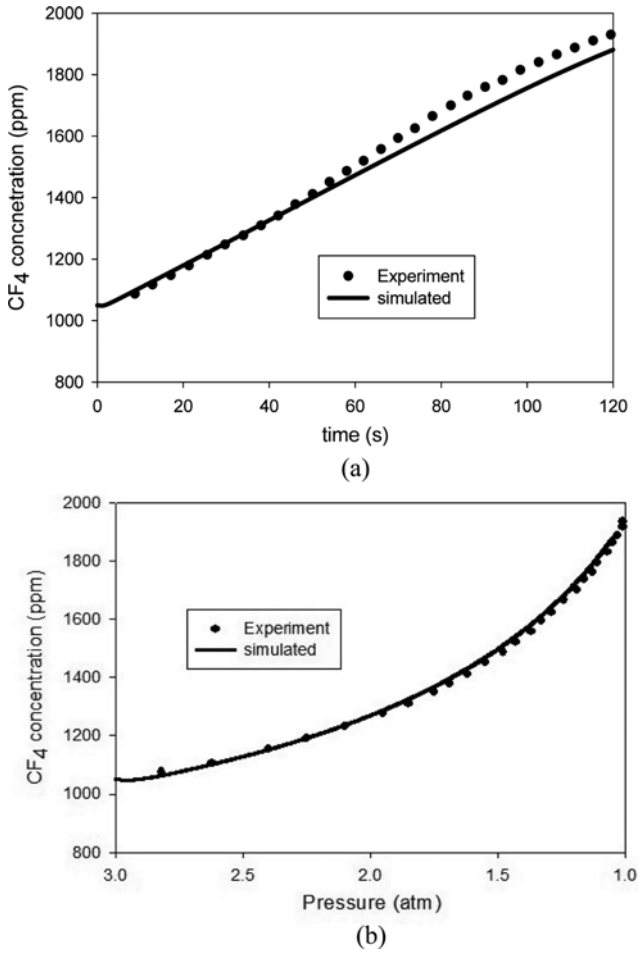

Fig. 7. Change in the CF_4 concentration during depressurization with (a) time and (b) bed pressure. The bed was saturated with 1,050 ppm of CF_4 before depressurization.

ping below the experimental values and reaching a maximum at 1,880 ppm. As shown in Fig. 6(a), the simulated pressure trend resembled the experimental one, but the absolute pressure values were not identical. The desorption of CF_4 was caused by adsorption bed pressure changes, necessitating the examination of CF_4 concentration changes as a function of adsorption bed pressure.

Fig. 7(b) shows the correlation between adsorption bed pressure and CF_4 concentration for depressurization from 3.0 atm to atmospheric pressure, with the CF_4 concentration increasing with decreasing pressure. This increase was slow at the initial depressurization stage, becoming faster with progressing depressurization, which implies that as the pressure dropped further, the amount of desorbed CF_4 per unit pressure change exceeded that of nitrogen. Fig. 7(b) compares the simulated CF_4 concentration changes to the experimental results, showing that these changes were successfully predicted for the entire pressure range. Therefore, it was concluded that the LDF approximation used for the simulation accurately predicted changes in the CF_4 concentration even for the depressurization step. The MTC proposed by Glueckauf [16] is given by $15(D_e/R_p^2)$, while Nakao and Suzuki [17] expressed MTC as a function of the dimensionless half-cycle time ($\theta_c=t_c(D_e/R_p^2)$). Based on the MTC derived from the simulated adsorption breakthrough curve, the

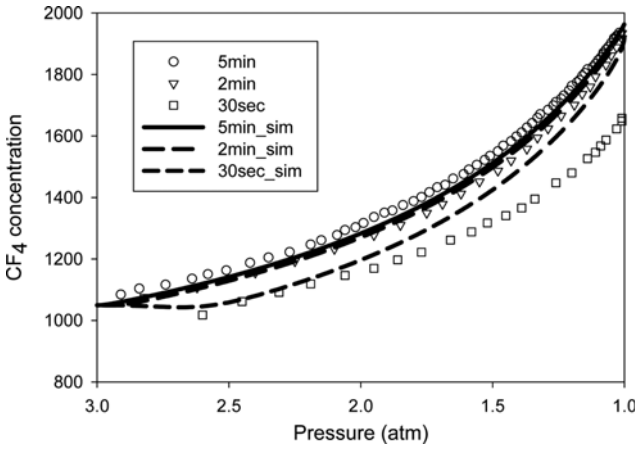

Fig. 8. Effect of depressurization time and bed pressure on the concentration of CF_4. The bed was saturated with 1,050 ppm of CF_4 before depressurization.

value of D_e/R_p^2 for CF_4 was determined as 3.33×10^{-3}. For a depressurization time of 120 s, θ_c equaled 0.4, and the MTC calculated as$15(D_e/R_p^2)$ for $\theta_c>1$ shows that it can be used to successfully model the actual mass transfer phenomenon.

CF_4 concentration changes were examined for depressurization times of 0.5, 2, and 5 min, with the results of this experiment and the corresponding simulation shown in Fig. 8. Experimental results reveal that the pressure-concentration curves obtained for depressurization times of 2 and 5 min showed similar trends. However, when depressurization lasted 30 s, the CF_4 concentration at any given pressure was slightly lower than that observed for 2-min and 5-min depressurizations, reaching ~1,670 ppm at the final depressurization pressure. This CF_4 concentration was significantly lower than the approximate value of 1,950 ppm obtained for 2-min and 5-min depressurizations. Fig. 8 also shows the simulated pressure-concentration changes, with very similar pressure-concentration curves observed for 2-min and 5-min depressurizations. However, a pressure-concentration curve distinctly different from those of 2-min and 5-min depressurizations was obtained for a 30-s depressurization. When the half-cycle time was substituted for depressurization time to calculate θ_c, values of 0.4 and 1.0 were obtained for 2-min and 5-min depressurizations, respectively, indicating that within this range of θ_c, the experimental pressure-concentration curves could be accurately modeled using the conventional term proposed by Glueckauf, i.e., $15(D_e/R_p^2)$ [16]. For a depressurization time of 30 s, θ_c equaled 0.1, with accurate modeling of adsorption and desorption phenomena possible using MTC=$15(D_e/R_p^2)$ according to Nakao and Suzuki [17]. However, as shown in Fig. 8, the simulation failed to accurately model experimental results in the case of a 30-s depressurization. The corresponding predictions for the initial depressurization stage (up to approximately 2 atm) were quite accurate, significantly deviating from experimental results as depressurization progressed further. This demonstrated that for a depressurization time of 30 s, the rate of CF_4 desorption predicted using the LDF approximation was faster than that obtained experimentally. According to Nakao and Suzuki [17], for $\theta_c=0.1$, the LDF approximation using $15(D_e/R_p^2)$ as the MTC accu-

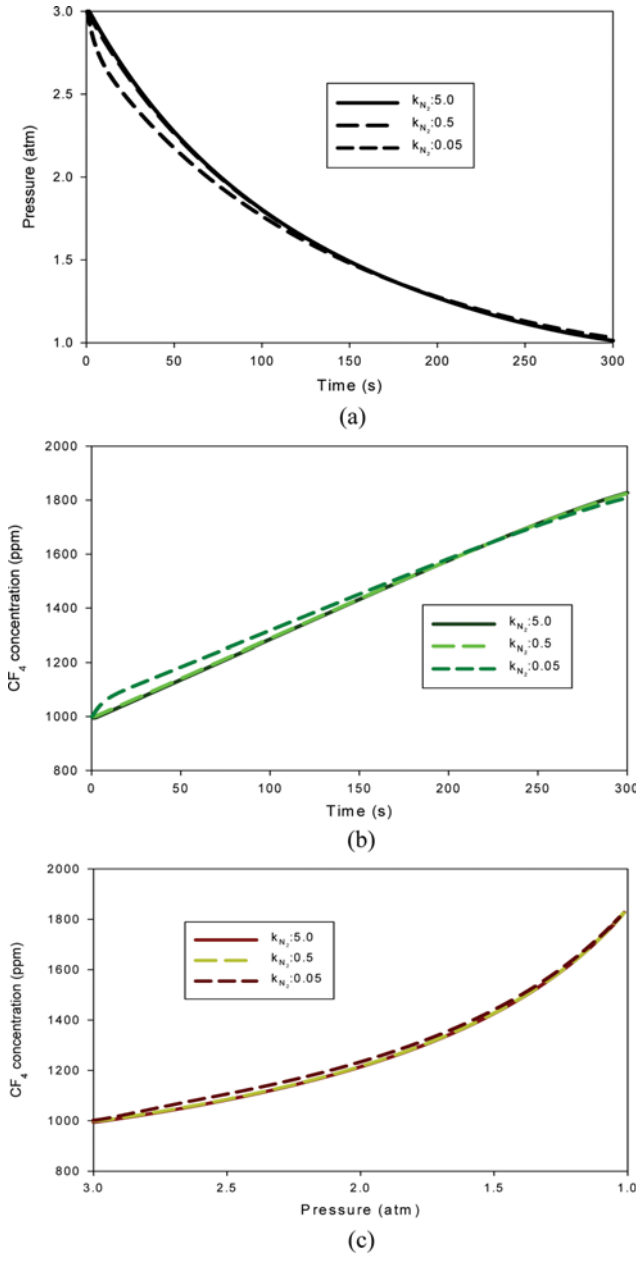

Fig. 9. Effect of N_2 mass transfer coefficient on the time dependences of (a) pressure (b) CF_4 concentration; (c) the effect of N_2 mass transfer coefficient on the pressure dependence of CF_4 concentration during depressurization from 3 to 1 atm (the bed was assumed to be saturated with 1,000 ppm of CF_4 before depressurization).

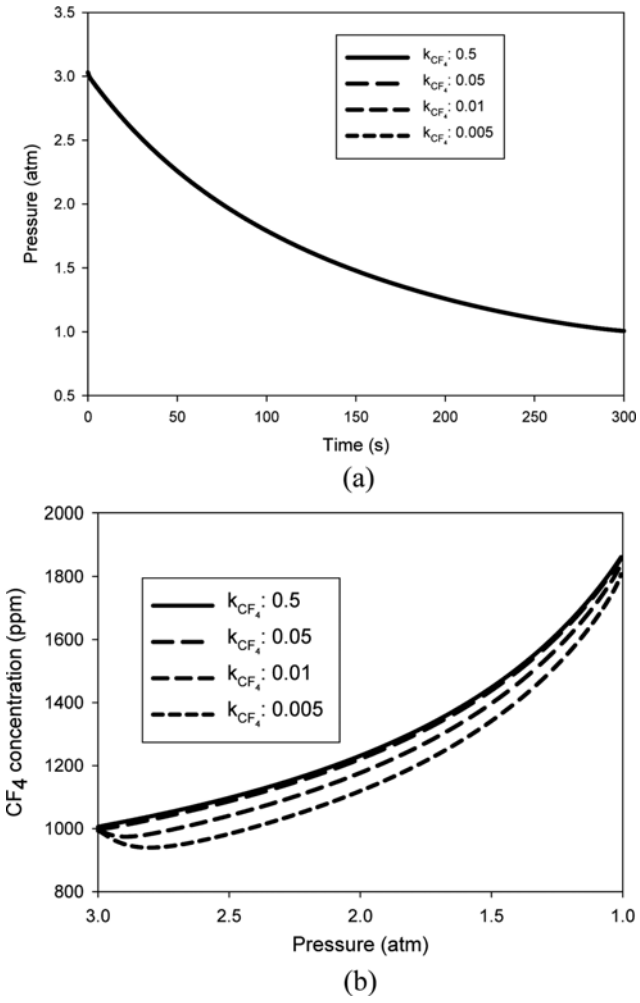

Fig. 10. Effect of CF_4 mass transfer coefficient on the dependence of CF_4 concentration on (a) time and (b) pressure during depressurization from 3 to 1 atm (the bed was assumed to be saturated with 1,000 ppm of CF_4 before depressurization).

rately predicted the cyclic steady state derived from the diffusion model, but failed to predict the concentration changes during the half-cycle of adsorption and desorption. Chahbani and Tondeur [23] compared changes in the concentration of strongly adsorbed species during pressurization and compression calculated using the diffusion model and the LDF approximation. According to their results, the concentrations of these adsorbates predicted using the LDF approximation were higher than the ones obtained using the diffusion model, even for $\theta_c \geq 0.1$. Based on the aforementioned results, even for $\theta_c \geq 0.1$, the values predicted using MTC=15(D_e/R_p^2) disagreed with experimentally determined ones.

The effects of MTC changes for N_2 and CF_4 during the depressurization step on CF_4 concentrations are shown in Figs. 9 and 10. Fig. 9(a) shows the pressure change during depressurization when the MTC of N_2 changed from 0.05 to 5.0 s^{-1}. The pressure changes were virtually the same for MTC values of 5 and 0.5 s^{-1}, but the pressure dropped more rapidly during the initial depressurization stage for MTC=0.05 s^{-1}. This was due to the desorption rate of N_2 being slow for MTC=0.05 s^{-1}, resulting in a small amount of desorbed N_2 in the gas phase during the initial depressurization stage. Fig. 9(b) shows the changes in the CF_4 concentration with depressurization time, with the trends for N_2 MTCs of 5.0 and 0.5 s^{-1} being very similar, whereas for an MTC of 0.05 s^{-1}, the concentration of CF_4 during the initial depressurization stage was higher than in the above two cases. As mentioned, this was due to the N_2 desorption rate being slow at an MTC of 0.05 s^{-1}, resulting in a reduced amount of desorbed N_2. However, the plot of CF_4 concentration change with pressure (Fig. 9(c)) showed that the MTC of N_2 did

not have a significant effect on the concentration of CF_4.

Fig. 10 shows the simulated effects of the MTC of CF_4 on its concentration during depressurization, obtained for 5-min depressurization of the adsorption bed saturated with 1,000 ppm of CF_4 from 3 atm to atmospheric pressure. Unlike the changes in the MTC of N_2 in Fig. 9(a), those of the MTC of CF_4 did not affect the trend of adsorption bed pressure change. Thus, the adsorption bed pressure changes remained the same even when the MTC of CF_4 changed from 0.005 to 0.5 s^{-1}, because the concentration of CF_4 in the mixed gas was low (several thousands of ppm), and the amount of desorbed CF_4 was not large enough to affect the pressure changes in the adsorption bed. Fig. 10 shows the changes in CF_4 concentration as a function of adsorption bed pressure, which were quite steady for the corresponding MTC values of 0.05 and 0.5 s^{-1}. This demonstrated that when the MTC of CF_4 was equal to or greater than 0.05 s^{-1}, the desorption rate reached equilibrium almost instantaneously during 5-min depressurization. However, when this parameter equaled 0.01 or 0.005 s^{-1}, the concentration of CF_4 dropped below the feed concentration of 1,000 ppm in the initial depressurization stage, increasing afterwards.

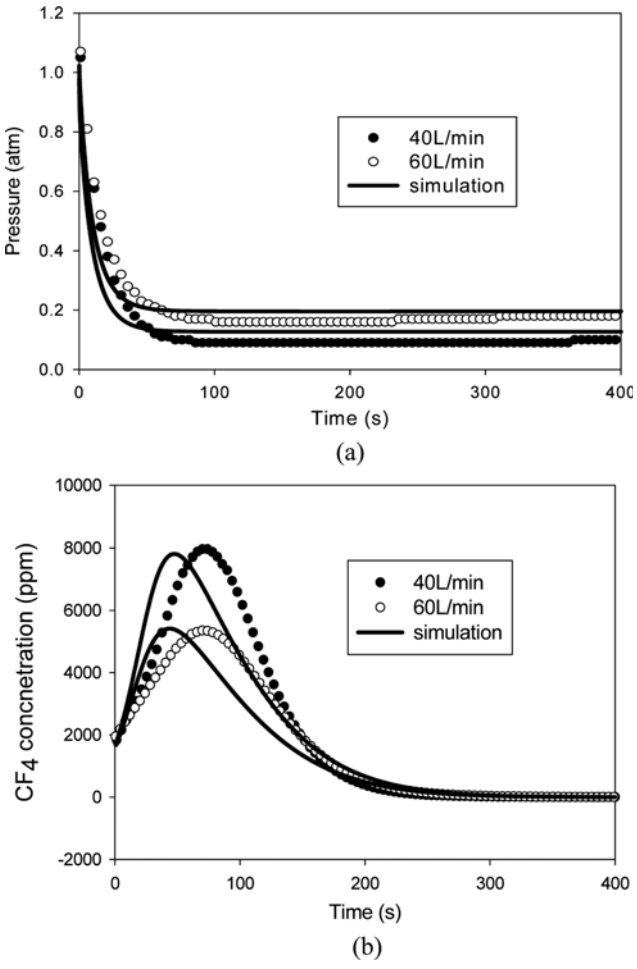

Fig. 11. (a) Pressure and (b) CF_4 concentration histories for various N_2 purge flow rates during the vacuum purge (the bed was saturated with 1,000 ppm of CF_4 at 3.2 atm and then depressurized to 1 atm in 30 s).

This is because the CF_4 desorption rate was much slower than that of N_2, causing CF_4 to be diluted by the desorbed N_2 in the initial depressurization stage.

4. Vacuum Desorption Experiments and Simulations

Fig. 11 shows pressure changes within the adsorption bed and changes in the CF_4 concentration in the desorbed gas observed in vacuum desorption experiments performed after saturating the adsorption bed with 1,000 ppm of CF_4 and depressurizing it from 3.2 atm to atmospheric pressure within 30 s. The above figure shows the results obtained for vacuum desorption with simultaneous N_2 purging (40 and 60 L/min). As shown in Fig. 11(a), the pressure dropped to ~0.1 atm for purging at 40 L/min and to 0.16 atm for purging at 60 L/min. The vacuum pump used in the experiment had a suction capacity of 600 L/min; however, a value of 350 L/min was used for simulations because of the possible pressure drop caused by the vacuum tube and valve. As a result (Fig. 11(a)), the minimum vacuum pressure corresponded to 0.13 atm for purging at 40 L/min and to 0.19 atm for purging at 60 L/min, being slightly higher than the experimental results. Despite this, the initial desorption pressures were lower than the experimental values for both purging rates. The inconsistent pressure trends can be explained by several reasons, including changes in the vacuum pump suction capacity with pressure, errors in predicting the possible amount of adsorbed N_2 using the IAS theory, and changes in the MTC of N_2 with pressure. The exact reason should be identified in further studies. Fig. 11(b) shows the changes in CF_4 concentration for vacuum desorption performed at N_2 purge rates of 40 and 60 L/min, with purging at 40 L/min, resulting in a roughly eight-fold increase in the CF_4 concentration, with a maximum of 8,000 ppm. Purging at 60 L/min resulted in a five-fold increase in the CF_4 concentration, with a maximum of 5,300 ppm. The simulated results were similar to the experimental ones, showing peak CF_4 concentrations of 7,800 and 5,400 ppm for purging at 40 and 60 L/min, respectively. The maximum CF_4 concentrations were observed when the vacuum pressure was at its minimum in both experimental and simulation analyses, but the time of the maximum CF_4 concentration in the experiment and simulation differed. The above findings demonstrate that accurate predictions of pressure changes are required to accurately model CF_4 concentration changes during vacuum desorption.

CONCLUSION

As a pre-step to designing an adsorption process for concentrating CF_4 from a mixture of CF_4/N_2, we examined the dynamics of CF_4 adsorption and desorption on activated carbon. In particular, a theoretical analysis of CF_4 desorption dynamics during depressurization was performed based on experimental data and simulations.

In this theoretical analysis, binary adsorption equilibria were predicted using the IAS theory, and the mass transfer rate of each component was calculated using the LDF approximation. This model accurately predicted adsorption breakthrough curves for CF_4 concentrations of 500-1,500 ppm and flow rates of 100-200 L/min, showing that the IAS theory could accurately predict the binary adsorption equilibria of CF_4 for a wide range of concentrations.

To understand the desorption dynamics during depressurization, changes in CF_4 concentration were analyzed during the depressurization of an adsorption bed saturated with 1,050 ppm of CF_4 from 3.0 atm to atmospheric pressure. Moreover, the corresponding concentration changes were simulated using the LDF model. The concentration of CF_4 increased slowly in the initial depressurization stage, rising faster as the pressure approached 1 atm. The effects of depressurization time on CF_4 concentration were studied for the corresponding values of 30 s, 2 min, and 5 min. Experimentally determined concentration changes were nearly identical for 2- and 5-min depressurizations, while the simulated CF_4 concentrations were higher than the experimental ones for 30-s depressurization. This result demonstrated that MTCs obtained from adsorption data were not directly applicable in the case of short depressurization times (θ_c<0.1).

The effects of N_2 and CF_4 MTCs (varied in the ranges of 0.05-5.0 s^{-1} and 0.005-0.5 s^{-1}, respectively) on CF_4 concentration during depressurization were studied by simulation. The MTC of CF_4 exhibited a significant effect on the concentration of the same in the desorbed gas. When the MTC of CF_4 was equal to or greater than 0.05 s^{-1}, the CF_4 concentration curves for 5-min depressurization were fairly unchanged. However, when this parameter equaled 0.01 or 0.005 s^{-1}, the concentration of CF_4 dropped below its feed concentration of 1,000 ppm during the initial stage of depressurization, increasing thereafter.

To characterize vacuum desorption, the adsorption bed was saturated with 1,000 ppm of CF_4 and depressurized from 3.0 atm to atmospheric pressure within 30 s. Subsequently, N_2 purging (40 and 60 L/min) was performed simultaneously with vacuum desorption to analyze the CF_4 concentration. Both experimental and simulated CF_4 concentrations increased roughly eight-fold for purging at 40 mL/min and approximately five-fold for purging at 60 L/min, with peak CF_4 concentrations observed when the vacuum pressure was at its minimum. However, the times when the CF_4 concentration reached its maximum were different, being shorter for simulated results. Thus, this study opens new ways of reducing PFC emissions and demonstrates that accurate prediction of pressure changes is important for precise modeling of CF_4 concentration changes.

ACKNOWLEDGEMENTS

This research was supported by the R&D center for Reduction of Non-CO_2 Greenhouse Gases (No. 2013001690014, Title: Development of high performance abatement technology for PFCs and NF_3 with high destruction rate and energy efficiency using excess enthalpy combustion with appropriate enrichment) funded by Korea Ministry of Environment.

SYMBOLS USED

a_{i1} : Langmuir isotherm parameter defined in Eq. (7) [mol/g]
a_{i2} : Langmuir isotherm parameter defined in Eq. (7) [mol·K/g]
b_i : Langmuir isotherm parameter defined in Eq. (6) [atm^{-1}]
b_{i0} : Langmuir isotherm parameter defined in Eq. (7) [atm^{-1}]
b_{i1} : Langmuir isotherm parameter defined in Eq. (7) [K]
C : total molar concentration [mol/m^3]
C_{pg}, C_{ps}, C_{pw} : gas, adsorbent, and wall heat capacities, respectively [cal/(g·K)]
D_e : effective diffusion coefficient [cm^2/s]
$-\Delta H_a$: average heat of adsorption [cal/mol]
h_w : heat transfer coefficient of the internal wall surface [cal/(cm^2·s·K)]
K_1, K_2 : ergun equation parameters defined in Eq. (8)
L : bed length [m]
p : total pressure [atm]
q_i : amount of adsorbed i^{th} component [mol/g]
q_{si} : parameter defined in Eq. (6) [mol/g]
R_g : gas constant [cal/(mol·K)]
P : pressure [atm]
P_{atm} : atmospheric pressure [atm]
R_p : adsorbent particle radius [cm]
T : absolute temperature [K]
T_F : feed temperature [K]
T_w : column wall temperature [K]
t : time [s]
u : superficial velocity [cm/s]
u_H : superficial velocity of feed [cm/s]
u_D : superficial velocity at bed outlet during depressurization [cm/s]
u_{PU} : superficial velocity of purge gas [cm/s]
u_{vac} : superficial velocity at bed outlet during vacuum purge [cm/s]
U_w : heat transfer coefficient at outer wall surface []
y_i : mole fraction of species [-]
z : axial distance in bed from the inlet
Z : height of packing [-]

Greek Letters

θ_c : half-cycle time [-]
ε : bed porosity [-]
ρ_g, ρ_p, ρ_w : gas, adsorbent, and wall densities, respectively [g/cm^3]

REFERENCES

1. J. Hou, W.-m. Sun, C.-m. Li, S.-h. Wang and H.-q. Hou, *J. Environ. Sci.*, **11**, 82 (1999).
2. M. T. Radoiu, *Radiat. Phys. Chem.*, **62**, 113 (2004).
3. H. M. Lee, M. B. Chang and R. F. Lu, *Ind. Eng. Chem. Res.*, **44**, 5526 (2005).
4. J. Sun and D. Park, *Korean J. Chem. Eng.*, **20**, 476 (2003).
5. Y. Takita, H. Wakamatsu, M. Tokumaru, H. Nishiguchi, M. Ito and T. Ishihara, *Appl. Catal. A: Gen.*, **194-195**, 55 (2000).
6. X.-F. Xua, J. Y. Jeon, M. H. Choi, H. Y. Kim, W. C. Choi and Y.-K. Park, *J. Mole. Catal. A: Chem.*, **266**, 131 (2007).
7. S. Suh, N. G. Ahn and B. Na, *Korean J. Chem. Eng.*, **25**, 1518 (2008).
8. S. Cho, S. Hong, J. Park, H. Beum and K. B. Lee, *Ind. Eng. Chem. Res.*, **54**, 8561 (2015).
9. L. Jiang, L. T. Biegler and V. G. Fox, *AIChE J.*, **49**, 1140 (2003).
10. J. Jee, J. Lee and C. Lee, *Ind. Eng. Chem. Res.*, **40**, 3647 (2001).
11. A. Malek and S. Farooq, *AIChE J.*, **44**, 1985 (1998).

12. J. Yang and C. Lee, *AIChE J.*, **44**, 1325 (1998).
13. J. Park, J. Kim and S. Cho, *AIChE J.*, **46**, 790 (2000).
14. R. T. Yang, *Gas separation by adsorption processes*, London Imperial College Press (1997).
15. M. S. Shafeeyan, W. M. A. Wan Daud and A. Shamiri, *Chem. Eng. Res. Design*, **92**, 961 (2014).
16. E. Glueckauf, *Transactions of the Faraday Society*, **51**, 1540 (1955).
17. S. Nakao and M. Suzuki, *J. Chem. Eng. Japan*, **16**, 114 (1983).
18. E. Alpay and D. M. Scott, *Chem. Eng. Sci.*, **47**, 499 (1992).
19. N. S. Raghavan, M. M. Hassan and D. M. Ruthven, *Chem. Eng. Sci.*, **41**, 2787 (1986).
20. C. H. Liaw, J. S. P. Wang, R. A. Greenkorn and K. C. Chao, *AIChE J.*, **25**, 376 (1979).
21. D. D. Do and P. L. J. Mayfield, *AIChE J.*, **33**(8), 1397 (1987).
22. J. Lee and D. H. Kim, *Korean J. Chem. Eng.*, **33**, 1186 (2016).
23. M. H. Chahbani and D. Tondeur, *Sep. Purif. Technol.*, **20**, 185 (2000).
24. Z. P. Lu, J. M. Loureiro, M. D. LeVan and A. E. Rodrigues, *Gas Sep. Purif.*, **6**, 15 (1992).
25. A. E. Rodrigues, J. M. Loureiro and M. D. LeVan, *Gas Sep. Purif.*, **5**, 115 (1991).
26. J. Hart, M. J. Battrum and W. J. Thomas, *Gas Sep. Purif.*, **4**, 97 (1990).
27. R. S. Todd and P. A. Webley, *AIChE J.*, **52**, 3126 (2006).